Landslide mapping from structure-from-motion analysis of photos acquired by a drone

Umair Asghar, Dwayne D. Tannant
School of Engineering, University of British Columbia, Kelowna, BC, Canada

ABSTRACT
Small drones equipped with cameras are an inexpensive alternative to lidar for mapping landslides. A ground control network is typically needed to achieve higher mapping accuracies. Complex natural environments often limit the ground control point (GCP) placement. Aerial photographs of a large slowly moving landslide involving multiple steep slopes and tree cover were acquired and processed using a structure-from-motion technique to produce a dense three-dimensional point cloud. The resulting point cloud was georeferenced with six different GCP configurations to test the influence of the number and the distribution of GCPs on mapping accuracies. Horizontal and vertical mapping accuracies of 58 mm and 44 mm, respectively, were achieved for the most accurate GCP configuration. The 3D change in the natural terrain over a 1-year period was also measured by comparing point clouds of the landslide generated from repeat photography. Movements of 0.4 m to over 1 m occurred at the toe of the landslide, whereas, other parts of the landslide either remained inactive or moved less than 0.1 m.

Les petits ronronnements équipés d'appareils photo sont une alternative peu coûteuse au lidar pour la cartographie des glissements de terrain. Un réseau de contrôle au sol est généralement nécessaire pour atteindre des précisions de cartographie plus élevées. Les environnements naturels complexes limitent souvent le placement du point de contrôle au sol (GCP). Des photographes aériennes d'un grand glissement de terrain à déplacement lent avec de multiples pentes abruptes et une couverture arborée ont été acquisées et traitées à l'aide d'une technique de structure à partir du mouvement pour produire un nuage de points tridimensionnels dense. Le nuage de points résultant ont été géoréférencé avec six configurations GCP différentes pour tester l'influence du nombre et de la distribution des GCP sur les précisions de cartographie. Des exactitudes horizontales et verticales de cartographie de 58 mm et 44 mm, respectivement, ont été obtenues pour la configuration GCP la plus précise. Le changement 3D du terrain naturel sur une période d'un an était mesuré en comparant les nuages de points du glissement de terrain générés à partir d'une photographie répétée. Des mouvements de 0,4 m à plus de 1 mètre se sont produits au bas du glissement de terrain, tandis que d'autres parties du glissement de terrain sont demeurées inactives ou se sont déplacées de moins de 0,1 m.

1 INTRODUCTION

The accuracy of drone-based mapping is important for its applicability in practice. Recent studies have shown that drone imagery processing that incorporates Structure from Motion (SfM) and Multiple View Stereopsis (MVS) image matching and point cloud densification algorithms can suffer from “bowl” or “doming” effects (a reprojection error) associated with the photographic network geometry (linear and parallel flight lines in most automated flights) and lens distortions in non-metric cameras. Additionally, off-nadir distortions are common because the flight altitude in most cases is low (50 to 150 m above ground) compared to traditional aerial photogrammetry (James and Robson, 2014; Peppa et al., 2016). An independent and accurate calibration of a drone-mounted camera can help to reduce or eliminate bowl-effects (James and Robson, 2014). Off-nadir and perspective distortions can also be reduced by ensuring a higher overlap (>75%) between images. However, even after eliminating these sources of error, spatial accuracy of a drone-SfM generated point cloud still depends on the accuracy of the georeferencing. Georeferencing can be done using camera locations captured by the GNSS GPS onboard the drone or by using ground control points measured on the ground and captured in the photographs. Incorporating a highly accurate compact RTK-GNSS receiver on a drone is very expensive and undermines the advantage of “low-cost” for drone-based mapping. Therefore, a network of ground control points (GCPs) that is relatively inexpensive and established with field measurements using a total station or RTK-GNSS is preferred.

Only a handful of studies have evaluated the influence of the number and the spatial distribution of GCPs on the precision of drone-SFM derived orthomosaics and digital surface models (DSMs) (Tahar, 2013; Shahbazi et al., 2015; Agüera-Vega et al., 2016; Tonkin and Midgley, 2016). In these studies, the mapping accuracy generally increased with an increasing number of GCPs that are well distributed on site. However, for complex natural environments, it is not always possible to place GCPs in a well-distributed configuration. For example, on very steep slopes it is usually unsafe to place GCPs directly on the slope. Similarly, tree cover not only limits the number and proper distribution of GCPs but also their visibility in a sufficient number of images. Compared to a flat terrain, a steep slope usually requires more GCPs to achieve equivalent mapping accuracies. Much of the published literature concerning indirect georeferencing dealt with flat or moderately sloping terrains with sparse to no vegetation cover, i.e., with few limitations on the number or the distribution of GCPs.

In this study, a landslide with highly variable topography and vegetation cover was studied. The topography and tree cover limited the number and the distribution of GCPs on the site. A low-cost rotary-wing drone was used to acquire aerial imagery in July 2016. The imagery was processed in a SfM-MVS workflow to generate a dense

point cloud. The influence of the number as well as the distribution of GCPs was assessed using six different GCP configurations. The influence of the topography and vegetation on the mapping accuracy was analyzed using a point cloud comparison technique. The landslide was mapped again in July 2017 using the same workflow to generate another point cloud. The point clouds from 2016 and 2017 were compared to detect movements over a one-year period. The results of the cloud comparison were verified by measuring the permanent GCP survey pins using an RTK-GNSS receiver.

2 STUDY SITE

The study site is a slow-moving landslide in the District of Summerland, British Columbia, Canada. The landslide is located on the northwest side of Trout Creek, and it is bounded by the Summerland Golf Club on the west and Canyon View Road on the north (Fig. 1). The landslide area is approximately 0.28 km^2. An earlier study of this landslide by Riglin (1977) noted that large landslide movements had occurred before 1938 and the main head scarp had progressed to its rough present-day location. Riglin (1977) classified the landslide failure mechanism as a retrogressive rotational slump with a backward tilt. Translational movements also occurred downslope resulting in depressed units or grabens at various locations. Riglin (1977) also mentions the flow of silt and sand mobilized by the groundwater discharging at the toe of the landslide, which continues to this day.

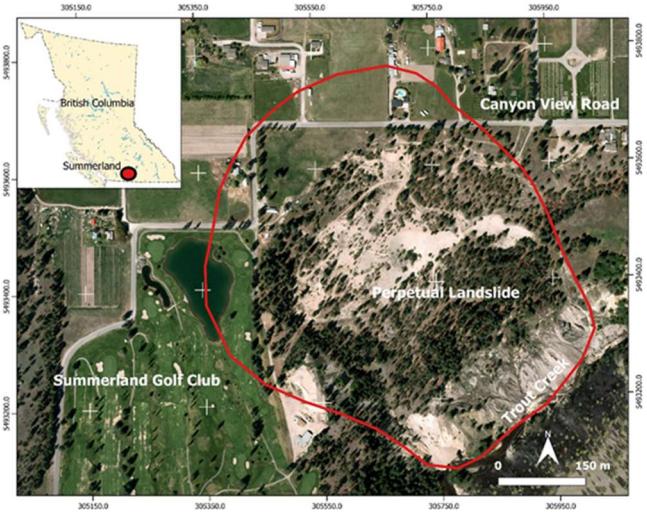

Figure 1. Location of the Summerland landslide

The landslide vegetation cover ranges from bare sand to shrubs and Douglas Fir and Ponderosa Pine trees. The topography of the site varies from gently undulating at the top (0.5-5% slopes) to extremely steep (>70%) at the Trout Creek canyon. The total change in elevation between the creek and the top of the landslide scarp is approximately 128 m.

3 AERIAL IMAGE ACQUISITION AND GCP SURVEY

A DJI Phantom 3 Advanced quadcopter was used to acquire images, and Pix4D Capture (Pix4D, 2016a) was used to establish the flight paths in a Grid Mission mode. For areas with steep slopes and dense tree cover, a high image overlap is needed with SfM techniques to extract maximum detail. Therefore, the frontal and side overlaps were set to 90% and 65%, respectively.

Four flights were made in 2016 to cover the whole landslide. The flight grids for 2016 showing camera positions are shown in Fig. 2. Three flights (Grids I to III) covering about 85% of the landslide were made at 70 m above take-off point. Because of varied site topography, the typical drone height above the ground during the flights for the three grids was roughly 60 to 90 m. The fourth flight represented by Grid IV in Fig. 3 was made at a 60 m take-off height to map the toe region of the landslide. Similarly, five flights (four at 80 m and one at 60 m above take-off point) were used in 2017 to cover the landslide.

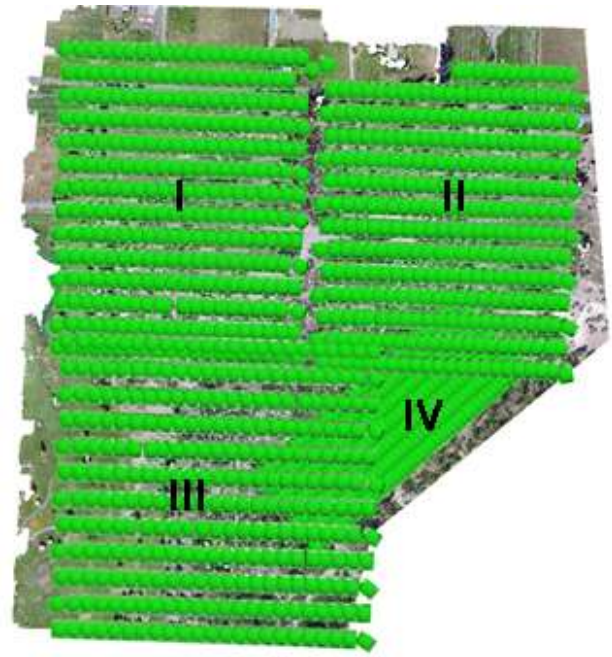

Figure 2. Flight paths and photo locations

The weather during the flights was sunny with some clouds, but there were significant differences in lighting and associated shadows on the ground due to tree cover in different parts of the landslide and delays between successive flights. The shutter speed of the camera was set to automatic, and ISO was fixed at 100 to avoid image noise. All images were acquired at an interval of 2 s. A total of 1160 and 945 images were acquired in the years 2016 and 2017, respectively.

A geodetic survey was performed a day before acquiring the aerial imagery in 2016 as well as in 2017. The purpose was to establish a ground control network to georeference the drone imagery and to independently measure movements of discrete points over time. The ground control network comprised of suitably selected

permanent features (four irrigation meters, a fire hydrant, two utility poles, and two concrete posts), temporary points spread across the landslide, as well as permanent steel rods inserted into the ground. All the points were measured with a Topcon GR-5 RTK-GNSS base station and a rover with ~5 cm accuracy.

Removable 0.6 m square plywood targets were placed and centred on top of the steel rod GCPs to facilitate the identification and marking of the GCPs in the photographs. Ideally, GCPs should be evenly distributed across the entire site. However, this was not feasible. The toe area of the landslide was not safely accessible, and GCPs were not placed in heavily treed areas because they could not be seen in a sufficient number of images.

4 IMAGE PROCESSING AND 3D POINT CLOUDS

The aerial imagery was processed in Pix4D Mapper Professional (Pix4D, 2016b) SfM software. Not all images acquired by the drone were used. Images with blur or false colour were discarded. The remaining images (1132 for 2016 and 912 for 2017) were loaded into Pix4D. The coordinates of the GCPs were also loaded as a text file.

The project was split into two subprojects for initial processing to avoid software problems. An initial point cloud was made using image geotags to improve the manual process of marking the GCPs in individual images. GCPs were marked semi-automatically in individual photographs using the ray cloud editor in Pix4D.

After marking GCPs, both subprojects were merged, and the rematch and reoptimize steps were run. Computation of the rotational and translational matrices as well as a scale factor to accurately georeference the point cloud was based on the selected GCP configuration.

The sparse initial point cloud was densified using a multiple scale option with an upper scale limit of half of the original image scale to compute a maximum number of 3D points in areas with dense tree cover while maintaining sufficient detail in areas without trees. Also, a minimum limit of 3 matches per point was used along with a matching window size of 7×7 pixels. The point density value was kept optimum, which resulted in a 4 cm resolution for the 2016 point cloud (Fig. 3) covering an area of approximately 0.66 km^2, and 3.7 cm resolution for the year 2017 point cloud covering an area of 0.41 km^2. The 2016 point cloud contained 53.4 million points, whereas, the 2017 point cloud contained 52.0 million points. The final step involved extraction and export of the DSM and orthomosaic at a resolution of 5 cm/pixel.

5 GROUND CONTROL NETWORKS

Table 1 lists the different GCP configurations that were used. The red dots in Fig. 4 show the locations of the GCPs. A total of 39 points were measured, and those that were not used as GCPs served as the checkpoints (CPs).

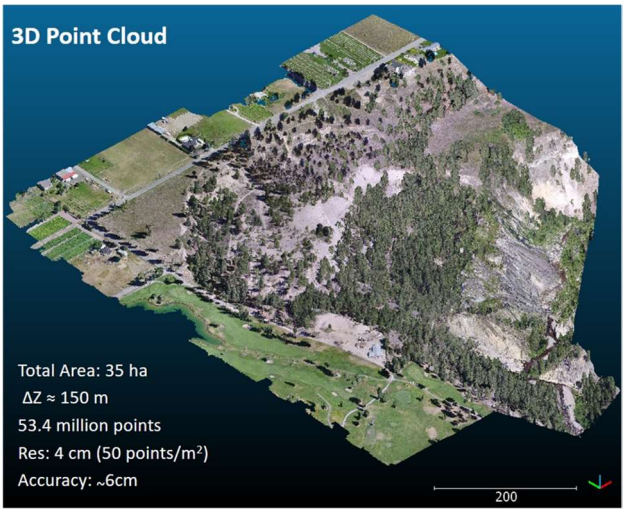

Figure 3. Point cloud of the Summerland landslide.

Table 1. GCP configurations used for georeferencing

	Description	GCPs
A	Widespread distribution	28
B	Most GCPs placed at the top and bottom of slopes on relatively flat benches	20
C	Evenly spread GCPs (grid-like distribution)	13
D	GCPs used in pairs	16
E	Modified D with only single GCPs used instead of pairs	8
F	Minimum number of GCPs used	5

6 ACCURACY ASSESSMENT

The accuracies of the DSM and the orthophoto are important for practical purposes, such as change detection, volume loss and accumulation measurements, slope profile generation, etc. For accuracy assessment, the difference (Δ) between the position of GCPs/CPs measured with the RTK-GNSS and their position computed from the orthomosaic and DSM were used to calculate the root mean square error (RMSE) in easting (X), northing (Y), horizontal (XY), and vertical (Z) directions.

For each GCP configuration, the GCP/CP position was manually marked on the orthomosaic, which was loading into ArcGIS 10.0. The use of the targets with the white dots helped to ensure accurate marking on the orthomosaic at an appropriate zoom level. A geometry calculation tool within ArcGIS was then used to compute the X-Y coordinates of the marked GCPs/CPs. The computed X-Y coordinates were then used to find the corresponding Z coordinates from the DSM using a point sampling tool in Quantum GIS. Table 2 shows the root mean square errors for each GCP configuration with respect to RTK-GNSS measurements.

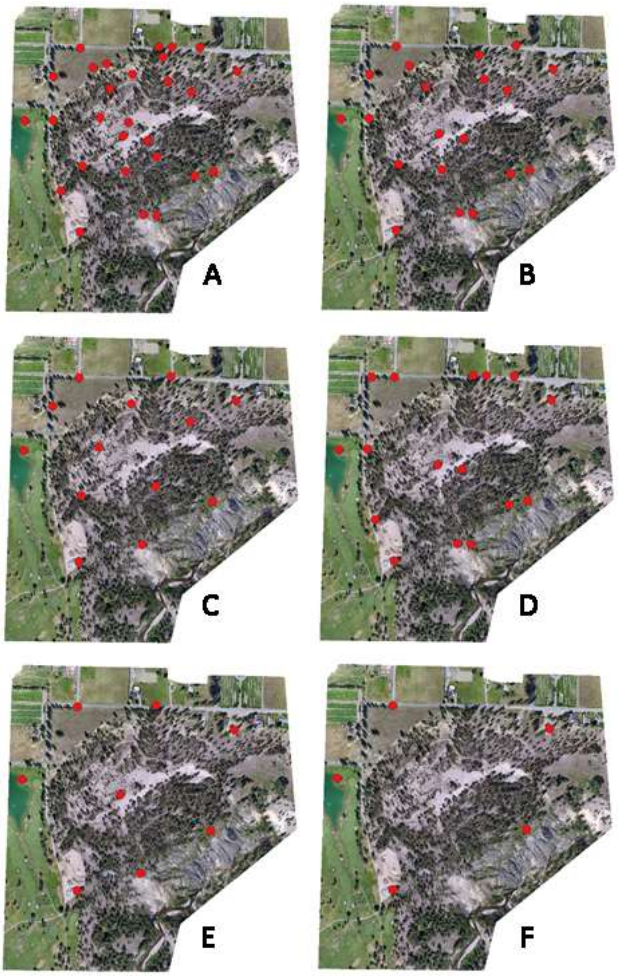

Figure 4. Different GCP configurations

Table 2. RMSE (mm) for computed GCP locations

	$RMSE_X$	$RMSE_Y$	$RMSE_{XY}$	$RMSE_Z$
A	42	40	58	44
B	47	33	57	51
C	66	46	80	93
D	70	53	88	115
E	66	53	85	111
F	140	85	164	241

Both horizontal and vertical accuracies increase with increasing number of GCPs, except for configuration B where the horizontal accuracy is slightly lower than that for configuration A. The RMSE in the X, Y, and Z directions increase from 42, 40, 44 mm for configuration A (28 GCPs) to 140, 85, 241 mm for configuration F (5 GCPs), respectively. In the horizontal plane, the RMSE in the X direction is higher than that in the Y direction. This could be associated with the east-west direction of the drone flights. Although the shutter speed was high (~1/600 to 1/1000 s), the drone speed (~3 m/s) causes some image blurring in the direction the drone was flown.

A reduction in GCPs affected the accuracy in the vertical direction more than the horizontal direction, which is agreement with the study conducted by Agüera-Vega et al. (2016). RMSE values for configurations A and B in all three directions are similar. For configuration B, eight GCPs mostly covering flat areas were removed from configuration A, and the remaining 20 GCPs were placed on relatively flat benches immediately above and below steep slopes. From an efficiency perspectives, configuration B used approximately 30% fewer GCPs compared to configuration A while maintaining similar accuracy. This careful reduction in the number of GCPs without significantly affecting the mapping accuracy is in agreement with Mancini et al. (2013) and Tonkin and Midgley (2016).

In configuration C, 13 GCPs were used such that the distance between the GCPs was approximately the same, and the GCPs were distributed in an arc-like grid. It is important to mention that a proper grid distribution of GCPs was not possible because of inaccessible areas and lack of visibility in dense tree cover. Configuration C did not result in the highest accuracy for the current study site, which is due to the variation in topography between GCPs. While a grid distribution produces good results for relatively flat terrain (Tonkin and Midgley, 2016), a configuration that takes into account all slopes (e.g., configuration B) is more likely to provide better results. The RMSE values for Configuration E came out to be slightly lower than Configuration D with double the number of GCPs. The difference in these two configurations is that in configuration D, 8 pairs of GCPs positioned relatively close to each other were used (7 pairs on landslide edges and 1 pair in the central area), whereas in configuration E, instead of pairs, only single GCPs were used. The shapes of both configurations were kept approximately similar. Finally, configuration F (5 GCPs) was used to test a minimal ground control configuration.

In addition to the number of GCPs, the mapping accuracy also depends on the distribution of GCPs with respect to the complexity of the environment. The results obtained in this study are in general agreement with other studies that report the effect of the number of GCPs on mapping accuracy. For example, Tahar (2013) increased the number of GCPs from four to nine in a grid configuration and concluded that both horizontal and vertical RMSE decreased from 490 and 830 mm for four GCPs to 450 and 770 mm for nine GCPs, respectively. Agüera-Vega et al. (2016) evaluated the variation in RMSE by using configurations of three, five and ten GCPs on five different terrains. On average, both horizontal and vertical accuracies increased from 225 and 100 mm for three GCPs to 53 and 49 mm for ten GCPs. Kršák et al. (2016) measured the height difference between UAV based and total station derived DSMs. Out of 237 measurements, only three points had a height difference greater than 120 mm, with an overall RMSE of 48 mm. Lindner et al. (2016) tested different configuration of GCPs and achieved RMSE in the vertical direction of 111 mm for 15 GCPs to 125 mm for 6 GCPs. Tonkin and Midgley (2016) conducted a comprehensive study in which 16 different distributions of

GCPs were tested. Horizontal and vertical RMSE varied from 59 and 45 mm for 101 GCPs to 156 mm and 126 mm for three GCPs.

Compared to many other studies that mapped landslides with UAV acquired imagery, the coordinate accuracy obtained in this study for configurations A and B was better. For example, when examining horizontal and vertical accuracies, Carvajal et al. (2011) achieved accuracies of 49 and 108 mm, and Lucieer et al. (2014) reported accuracies of 70 and 60 mm. Niethammer et al. (2012) achieved RMSE values of 500 and 310 mm in the horizontal and vertical directions while Lindner et al. (2016) achieved RMSE in the vertical direction of 111 mm. Accuracies obtained by Turner et al. (2013), i.e., 40 to 50 mm in horizontal and 30 to 40 mm in vertical directions, are better than the current study, however, they used a higher number of GCPs on a smaller area, and flew their UAV at a lower elevation (i.e., 40 m compared to 70 to 80 m in this study). Also, the topography was not as complex as the current study site. Peternel et al. (2016) achieved accuracies of 30 to 40 m in the horizontal and 20 to 30 m in the vertical directions, which are also better than that obtained in this study.

7 CHANGE DETECTION

The UAV images obtained in July 2017 were processed using GCP configuration A. The RMSE values for the July 2017 point cloud were calculated using the same workflow described earlier. The RMSE values in X, Y, and Z directions, respectively, were 59, 42, and 62 mm. Thus the accuracy of the July 2017 point cloud was slightly less than the July 2016 point cloud.

To detect the 3D changes in the natural terrain between July 2016 and July 2017, the point clouds from the two years were first filtered using a Cloth Simulation Filter (Zhang et al., 2016) to obtain bare earth points clouds. A ground offset distance of 0.3 m was used to differentiate vegetation from the ground points. The purpose of classification was to avoid errors in co-registration induced by variations in the vegetation. Since the two point clouds were constructed and georeferenced using separate workflows, co-registration is a necessary step before cloud comparison to avoid misalignments and rotational or scale differences. In CloudCompare (v2.8), the two point clouds were first masked to ensure they fully overlapped. Second, those parts that fall outside the active landslide area were segmented from both point clouds. These non-active parts were then co-registered using the Iterative Closest Point (ICP) algorithm to obtain the transformation matrix. Finally, this transformation matrix was applied to the July 2017 point cloud (aligned) to co-register it with the July 2016 point cloud (reference).

Once the point clouds were co-registered, they were compared using the M3C2 algorithm (CloudCompare plugin) to compute signed (and robust) distances directly between the two point clouds. The result of the M3C2 cloud comparison is shown in Fig. 5. The 3D displacement vectors at each of the fixed GCPs are also shown on top of the cloud comparison diagram. The figure shows that most of the landslide movement over the one-year period occurred in the toe region, where the measured distances vary from ±0.4 m to over ±1.0 m. This movement was consistent with the displacement vectors measured independently for the GCPs.

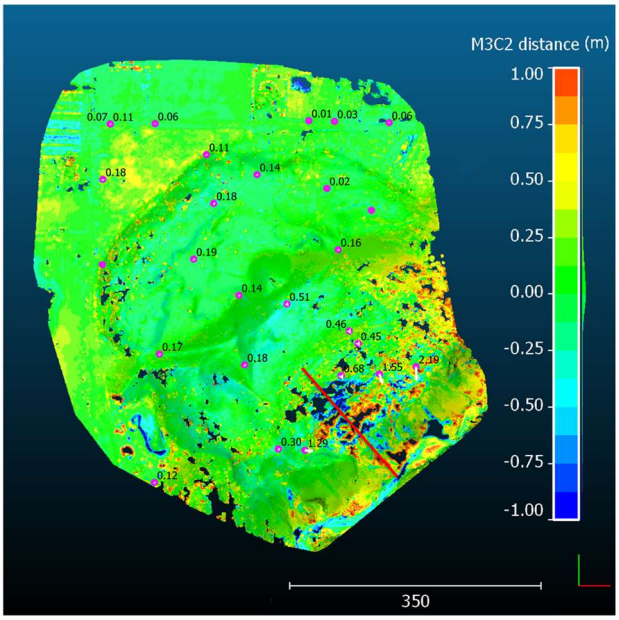

Figure 5. M3C2 map of 3D movements between July 2016 and July 2017 point clouds and displacement at each GCP from 2016 and 2017 RTK-GNSS measurements

Vertical profiles that were taken along the red line shown in Fig. 5 are shown in Fig. 6 for 2016 and 2017. Areas where the ground surface dropped can be seen upslope of areas where the ground surface has risen, indicating a displacement of the landslide materials between these locations.

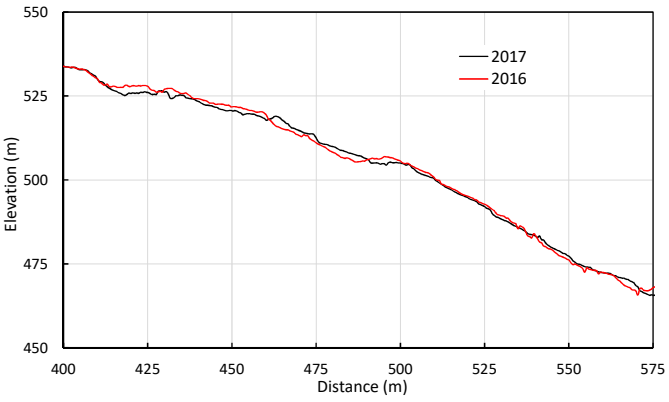

Figure 6. Vertical profile along the lower part of the landslide for July 2016 and July 2017

There are areas in the west and north-west of the landslide where the M3C2 distances show a movement in the range of ±0.5 m. However, this part of the landslide did not move more than 0.1 to 0.2 m based on a few independent measurements. The reason for differing displacement vectors and the higher M3C2 distance is that

in July 2017 the grass on the edge of the golf course and the crops in the fields were taller and denser in some areas and shorter in others compared to July 2016. The point cloud classification algorithm includes the grass/crops in the bare-earth point clouds by incorrectly classifying short thick vegetation as ground points. Therefore, a variation in vegetation height can induce errors in the change detection even after vegetation filtering.

8 CONCLUSION

In this study, a low-cost quadrotor drone equipped with a 12.4-megapixel digital camera was used to map and monitor the slow-moving Summerland landslide. The drone acquired aerial imagery was processed in a SfM based software package to generate a 4 cm resolution 3D point cloud containing over 53 million points with an average density of 28 points per m^3 after vegetation was removed. GCPs measured in the field with RTK-GNSS were used to georeference the point cloud in a UTM coordinate system. To assess the effect of the number and distribution of GCPs on the mapping accuracy, six different GCPconfigurations were tested. The RMSE errors in different directions were calculated by subtracting the 3D coordinates of the GCPs read from the orthophoto (for X and Y) and the DEM (for Z) from their location measured in the field using an RTK GNSS. The analysis revealed that the mapping accuracies are affected by both the number and the distribution of GCPs. Horizontal and vertical accuracies increased with increasing number of GCPs. However, if the GCPs are placed at transition points between flat and steep ground, the number of GCPs can be reduced while maintaining horizontal and vertical accuracies of 60 mm or better.

The 3D change in the natural terrain over a 1-year period from July 2016 to July 2017 was measured by comparing point clouds generated using imagery taken one year apart and using a cloud comparison technique. Movements in the range of ±0.4 m to over ±1 m occurred at the toe of the landslide. Other parts of the landslide either remained inactive or moved less than 0.1 m. These values were confirmed using the 2016 and 2017 positions of the permanent GCPs installed in the landslide and measured with an RTK GNSS system.

Simple drone imagery combined with the SfM technique can produce highly accurate (decimetre level) and multitemporal point clouds, DSMs, DEMs, and orthophotos for a complex terrain containing steep slopes covered with vegetation. Multi-temporal point clouds obtained using the drone-SfM technique can be used to map 3D landslide movements with decimetre accuracy. This is different from other landslide monitoring studies that compare DSMs/DEMs for indications of elevation change or orthophotos that provide horizontal translations. 3D movement can be mapped directly using the point clouds.

ACKNOWLEDGEMENTS

The authors thank the District of Summerland for providing access to the site. Some funding for this research came from Mitacs and the BC Oil and Gas Commission as a component of a study to improve methods to characterize stream crossings for pipeline design.

REFERENCES

Agüera-Vega, F., Carvajal-Ramírez, F., and Martínez-Carricondo, P. 2016. Accuracy of digital surface models and orthophotos derived from unmanned aerial vehicle photogrammetry, *J. of Surveying Eng.*, 04016025.

Carvajal, F., Agüera, F., and Pérez, M. 2011. Surveying a landslide in a road embankment using unmanned aerial vehicle photogrammetry, *Int. Archives of the Photogrammetry, Remote Sensing and Spatial Information Sciences, Vol. XXXVIII-1/C22*, 201-206..

James, M.R., and Robson, S. 2014. Mitigating systematic error in topographic models derived from UAV and ground-based image networks, *Earth Surface Processes and Landforms*, 39, 1413-1420.

Kršák, B., Blišťan, P., Pauliková, A., Puškárová, P., Kovanič, Ľ., Palková, J., and Zelizňaková, V. 2016. Use of low-cost UAV photogrammetry to analyze the accuracy of a digital elevation model in a case study, *Measurement*, 91, 276-287.

Lindner, G., Schraml, K., Mansberger, R., and Hübl, J. 2016. UAV monitoring and documentation of a large landslide, *Applied Geomatics*, 8, 1-11.

Lucieer, A., de Jong, S., and Turner, D. 2014. Mapping landslide displacements using structure from motion (SfM) and image correlation of multi-temporal drone photography, *Progress in Physical Geography*, 38, 97-116.

Mancini, F., Dubbini, M., Gattelli, M., Stecchi, F., Fabbri, S., and Gabbianelli, G. 2013. Using unmanned aerial vehicles (UAV) for high-resolution reconstruction of topography: the structure from motion approach on coastal environments, *Remote Sensing*, 5, 6880-6898.

Niethammer, U., James, M.R., Rothmund, S., Travelletti, J., and Joswig, M. 2012. UAV-based remote sensing of the Super-Sauze landslide: evaluation and results, *Engineering Geology*, 128, 2-11.

Peppa, M., Mills, J., Moore, P., Miller, P., and Chambers, J. 2016. Accuracy assessment of a UAV-based landslide monitoring system, *ISPRS-Int. Archives of the Photogrammetry, Remote Sensing and Spatial Information Sciences*, 895-902.

Peternel, T., Kumelj, Š., Oštir, K., and Komac, M. 2016. Monitoring the Potoška planina landslide (NW Slovenia) using UAV photogrammetry and tachymetric measurements, *Landslides*, 14, 395-406.

Riglin, L.D. 1977. The Perpetual Landslide Summerland, British Columbia, MSc Thesis, University of British Columbia.

Shahbazi, M., Sohn, G., Théau, J., and Menard, P. 2015. Development and evaluation of a UAV-photogrammetry system for precise 3D environmental modeling, *Sensors*, 15, 27493-524.

Tahar, K. 2013. An evaluation on different number of ground control points in unmanned aerial vehicle photogrammetric block, *ISPRS J. Photogramm. XL-2 (W2)*, 93-98.

Tonkin, T.N., and Midgley, N.G. 2016. Ground-control networks for image based surface reconstruction: an investigation of optimum survey designs using UAV derived imagery and structure-from-motion photogrammetry, *Remote Sensing*, 8, 786.

Turner, D., Lucieer, A., and Wallace, L. 2013. Direct georeferencing of ultrahigh-resolution drone imagery, *IEEE Transactions on Geoscience and Remote Sensing*, 52, 2738-2745.

Zhang, W., Qi, J., Wan, P., Wang, H., Xie, D., Wang, X., and Yan, G. 2016. An easy-to-use airborne LiDAR data filtering method based on cloth simulation, *Remote Sensing*, 8, 501.